(Received 17 January 2026, Accepted 11 February 2026, Scheduled 11 March 2026)

Mode Analysis for Prediction of Heating Patterns in Microwave Cavities Powered by Magnetron

Freda Carvalho[1, 2, *], Ashwini Kotrashetti[1, 2], and Kaustubh Bhattacharyya[1, 3]

[1] *Department of Electronics & Communication Engineering, Assam Don Bosco University, Guwahati, India*
[2] *Department of Electronics & Telecommunication Engineering, Don Bosco Insititute of Technology, Mumbai, India*
[3] *Department of Electronics, Assam Skill University, Guwahati, India*

ABSTRACT: Microwave heating, widely employed in the food industry, offers significant advantages due to its volumetric heating capabilities. However, its efficiency is often hindered by nonuniform heating patterns. This study aims to analyse heating patterns in a rectangular, single-fed domestic microwave oven, leveraging cost-effective methodologies. Theoretical analyses, electromagnetic simulations, and experimental measurements were conducted to characterise the resonant modes within an empty cavity and with a load. The mathematical computation of multiple-mode superposition within the cavity was performed for two domestic microwave ovens. Mathematical and experimental analyses demonstrate a close agreement in results. The findings reveal that mode distribution, influenced by cavity dimensions, load properties, load placement, and magnetron characteristics, significantly impacts heating patterns. This study helps us understand that in spite of the dynamic nature of the magnetron, it is important to superimpose multiple resonant modes prevalent within the cavity to understand influences on the microwave heating pattern of any food materials.

1. INTRODUCTION

Microwave heating has gained interest across industrial and domestic sectors due to its efficiency, rapid processing, and volumetric heating characteristics. Industries using microwave heating often cite nonuniform heating as a concern [1, 2]. Many efforts have optimized the heating of food products, differing for every sample under test (SUT) [3–8]. Domestic microwave ovens face nonuniform heating since they heat various SUTs and serve multiple purposes like preheating, cooking, defrosting, etc. [9–12]. Currently, the market features two main generator technologies: the traditional magnetron and the modern solid-state variant. Researchers have been analyzing heating patterns made by magnetrons. In a study by Birla et al. [13], the simulated and experimental heating patterns for frequencies of 2.42 GHz, 2.46 GHz, and 2.52 GHz within a domestic microwave oven matched. While the research details the return loss of the cavity, it does not provide insights into modes that contribute to generating particular heating patterns. Luan et al. [14] explored the frequency distribution variability among four domestic microwave ovens driven by magnetrons. The research highlights how magnetron aging leads to various heating patterns. Although these ovens are for domestic use, their dimensions and associated resonant frequencies must be considered to accurately describe heating behaviours, since domestic ovens have different dimensions. Zhou et al. [15] compare magnetron and solid state generator systems, where solid state generators create defined heating patterns in food due to their spectral purity. In a study by Zhou et al. [16], modes within cavities using solid-state generators are examined alongside experimental findings that match simulation results. This relationship is significant, as these generators show narrow bandwidth and selective mode excitation within the cavity. However, there remains a gap in exploring the type and number of modes in a magnetron-based cavity, which could yield valuable insights. Investigations into nonuniform heating often overlook cavity dimensions, failing to recognize the importance of resonant modes. The count of these modes is linked to the cavity's dimensions and must be a multiple of the wavelength at operational frequency. Increasing modes can aid in achieving more even heat distribution [17]. Magnetrons offer a wider bandwidth of around 70 MHz causing excitation of multiple modes [15]. This nature justifies their use in the food industry, where loaded cavities can accommodate more modes to treat food material [18]. Both magnetron and solid-state generators have their significance, suggesting potential coexistence in the future. Studies show that solid-state technology can address challenges of nonuniform heating seen with magnetron applications. However, market analysis shows that magnetrons maintain higher radio frequency (RF) power conversion efficiency than solid-state generators. Manufacturers continue efforts to reduce solid-state systems' cost per watt to compete with magnetron pricing [19]. While research exists on magnetron frequency shifting, systematic investigation of modes contributing to heating patterns in magnetron-based cavities remains lacking.

In the literature, heating patterns and mode distributions are examined post-heating through thermal imaging [20] and the bead pull technique, which identifies frequency shifts to outline resonance mode profiles during the heating process [21]. Additional methodologies employed during the heating process

* Corresponding author: Freda Carvalho (carvalhofreda@gmail.com).

TABLE 1. Comparison of methods used in literature to analyse modes during microwave heating.

Method	Equipment cost	Setup complexity	Why is it cost-effective?
Thermal Paper [24]	<$50	Low	No electronics, calibration, or entry to cavities beyond simple positioning; minimal risks are associated with brief exposures.
Bead Pull Perturbation [21]	$100–$500	Medium	Involves mounting a dielectric bead on a motorized linear stage, inserting it precisely through a small cavity hole, and syncing with a VNA to track frequency shifts while scanning.
Field Probe [25]	$500–$3000	High	A slender, open-ended coaxial probe supplied through a waveguide positioned below the cutoff frequency, an accurate motorized XYZ scanner for non-contact.
IR Thermography [14]	$1000+	Low	Rapid in performance, yet the camera is the most expensive option, suitable for swift oven evaluations, assuming optimal surface visibility.

encompass temperature and power intensity mapping via fiber-optic sensors [22], as well as the utilization of reversible thermal paint to generate thermal maps within the microwave cavity [23]. These techniques facilitate the visualization of mode patterns within microwave ovens. An analysis of equipment costs and setup complexities reveals that the thermal paper plotting method is more economical for budget-conscious laboratories than the other methods. As illustrated in Table 1, various reported methods are compared for cost-effectiveness.

In this study, the authors employ established methodologies to verify the frequencies generated by magnetrons in domestic ovens [13–15]. By analyzing the frequency distributions of magnetrons, one gains insight into resonant modes, facilitating the identification of optimal couplings of suitable mode distributions. These insights are crucial for the mathematical application and superimposition of the contained resonant modes, thereby reinforcing the validity of the experimental outcomes. Recent stirrer designs, such as anchor paddles and hybrid rigid-flexible paddles, enhance liquid heating uniformity but may not be as effective with solids [6, 26]. This study aims to predict microwave heating patterns for magnetron-powered ovens, particularly when mode stirring is impractical for solid materials or in conveyor-type microwave systems. This approach is intended to enhance food safety and ensure proper handling during batch processing. The authors propose that in large cavities equipped with multiple spaced magnetrons, it is possible to evaluate and superimpose the frequency distributions of each magnetron, thus predicting the resultant heating patterns within these environments. However, this study is limited to single-fed cavities. The following sections establish a theoretical framework for the resonant modes, informed by the cavity dimensions as detailed in Section 2. Section 3 offers a comprehensive description of the materials employed, alongside the methodologies and procedural steps relevant to the study. Furthermore, Section 4 elucidates the results of the electromagnetic (EM) simulations, which corroborate the experimental findings discussed in Section 5. The experimental results are presented in two phases: the measured frequencies and corresponding thermal paper plots. The thermal paper plots were validated through the mathematical analysis for the empty cavity and EM simulation for the loaded cavities.

2. MICROWAVE CAVITY HEATING FUNDAMENTALS

Domestic microwave ovens are enclosed metallic cavities utilized for microwave heating, which effectively confine electromagnetic fields within metallic boundaries. The resulting standing wave patterns generate maxima and minima of the fields at various locations, thereby creating modes within the cavities, as demonstrated in Equation (1).

$$E_i = E_o \left[\cos\left(\frac{m\pi X}{W}\right)\cos\left(\frac{n\pi Y}{L}\right)\sin\left(\frac{p\pi Z}{D}\right)\right] \quad (1)$$

In this context, variables m, n, and p denote half-wavelength variations of the electric or magnetic field across the dimensions of the rectangular cavity: width (W) along the X-axis, length (L) along the Y-axis, and depth (D) along the Z-axis. Symbol E_o represents the peak amplitude of the microwave source [17]. The electric field E_i induces a variable voltage stress within the load situated inside the cavity walls. Rectangular cavities, which exceed the operational wavelength, facilitate easier sample loading and enclosure while promoting the occurrence of multiple modes. The cutoff frequencies or resonant frequencies (f_r) of the modes within a rectangular cavity are determined by Equation (2).

$$f_r = \frac{1}{2\sqrt{\mu_0\epsilon_0}}\sqrt{\left(\frac{m}{W}\right)^2 + \left(\frac{n}{L}\right)^2 + \left(\frac{p}{D}\right)^2} \quad (2)$$

A schematic of an oven is shown in Figure 1, and the magnetron is provided with a DC or AC power (P_i). The microwave energy (P_s) is fed to the cavity in certain bands of microwave frequencies, and (P_r) represents reflected power, which depends upon the coupling of the power to the cavity and SUT. The material properties of SUT influence heating distribution, and various factors must be taken into account to ensure the optimal

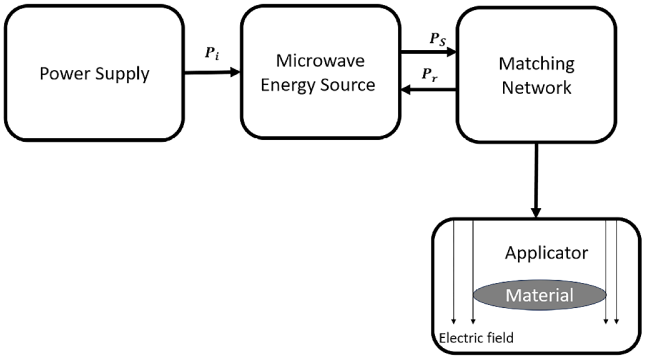

FIGURE 1. Schematic diagram of microwave oven [27].

performance of microwave heating cavities, which collectively contribute to the overall system efficiency (η_S). They include applicator efficiency, defined as the ratio of power deposited (P_d) in the dielectric that is placed inside a cavity to the input power, whereas there could be power reflected back at the source, termed as (P_r). Here, P_d in the dielectric is primarily due to dielectric losses (ϵ_r'') given by Equation (3) [17].

$$P_d = 2\pi f \epsilon_o \epsilon_r'' E_i^2 \tag{3}$$

From Equation (3), it is evident that an increase in the electric field E_i, which induces voltage stress in the load, leads to an elevation in P_d. The corresponding E_i of the cavity modes, as clearly demonstrated through Equations (1) and (2), is influenced by its dimensions. Additionally, the position of the magnetron, the placement of the load, and the types of load also play significant roles [19, 28]. In a 2009 study, Monzó-Cabrera et al. [3] examined the relationship between return loss and cavity efficiency, highlighting the optimal placement of the load in a domestic oven to achieve the best average temperature rise for samples.

To analyze the impact of the dielectric properties of the sample under test (SUT) on P_d, this study investigates a bread sample using the validated models from Weng et al. [29]. The model, as depicted in Equations (5) and (6), is influenced by frequency (f), moisture content (w), and temperature (T), which affect both the real (ϵ_r') and imaginary (ϵ_r'') components of dielectric permittivity. Effective heating necessitates dimensions similar to "D_{depth}", which decreases with an increase in frequency and dielectric losses, as demonstrated in Equation (4).

$$D_{depth} = \frac{\lambda\sqrt{\epsilon_r'}}{2\pi\epsilon_r''} \tag{4}$$

where λ is the wavelength for the given frequency of operation.

$$\begin{aligned}\frac{1}{\epsilon_r'} &= 1.236 - 0.00136 \times T + 0.0959 \times \log(f) \\ &\quad -0.0289 \times w + 0.000194 \times T \times \log(f) \\ &\quad -0.00626 \times \log(f)^2 + 0.000307 \times T \times w \end{aligned} \tag{5}$$

$$\begin{aligned}\log(\epsilon_r'') &= -8.366 + 0.136 \times T + 0.336 \times w \\ &\quad -0.716 \times \log(f) + 0.0000507 \times T^2 \\ &\quad +0.0793 \times \log(f)^2 - 0.00369 \times T \times \log(f) \\ &\quad -0.00291 \times T \times w - 0.0137 \times \log(f) \times w \end{aligned} \tag{6}$$

The power deposited in the bread sample increases at a constant moisture content of $w = 35\%$ and a fixed frequency of $f = 2450$ MHz, as evidenced by the increase in the electric field shown in Figure 2.

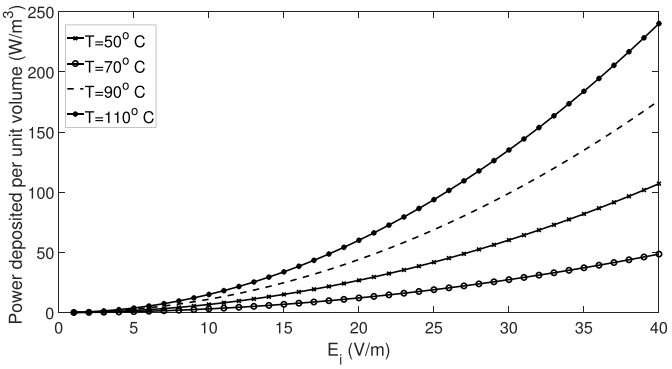

FIGURE 2. Power deposited in 1 kg of bread vs E_i (V/m) at frequency of 2450 MHz and moisture level.

2.1. Electrical Equivalent Model

The cavity is represented as an admittance form Foster network, as depicted in Figure 3. In this model, each shunt leg comprises a series element consisting of R_k, L_k, and C_k, which resonate at the mode frequency, (f_k). At the resonant frequency, a mode is established within the cavity, generating a specific field pattern. A total of 'N' modes exist within the operating bandwidth. The equivalent circuit depicts 'k' number of resonant modes inside a cavity, where $k = 1, 2, 3, ..., N$. Each of the shunt elements R_k, L_k, C_k corresponds to a resonant frequency, which is represented by Equation (7), and these resonant frequencies f_k occurring within the band can also be expressed by Equation (2), on the basis of cavity dimensions [17].

$$f_k = \frac{1}{2\pi\sqrt{L_k C_k}} \tag{7}$$

The characteristic impedances of TE and TM modes are expressed as in Equation (8).

$$Z_{ok} = \sqrt{\frac{L_k}{C_k}} \tag{8}$$

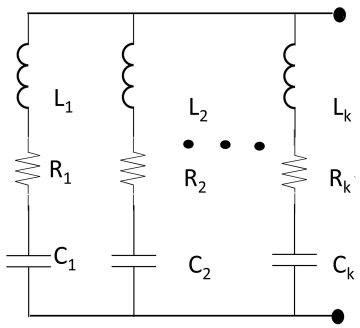

FIGURE 3. Equivalent circuit of a resonant cavity with k modes within a specified band.

TABLE 2. Parameters of Oven 1 and Oven 2.

Parameter	Oven 1	Oven 2
Model	SAMSUNG Model *MW73AD-B/XTL*	IFB 24PM2B model
Manufacture year	2017	2024
Power	800 W	900 W
Frequency	2450 MHz	2450 MHz
Cavity Volume	2450 MHz	2450 MHz
Volume	0.0165 m^3	0.0165 m^3
Dimensions	280 mm × 310 mm × 190 mm	280 mm × 310 mm × 190 mm

The L_k and C_k values change based on the mode type and how close the mode is to the cut-off frequency. There are two types of characteristic impedance: TE and TM modes. All excited modes should be far from their cut-off frequencies. The characteristic impedance of TE and TM modes at f_k can also be expressed using f_k and the induced signal frequencies $f_{s,k}$ as shown in Equations (9) and (10) [17].

$$Z_{TM} = \sqrt{\frac{\mu_o}{\epsilon_o}\left[1-\left(\frac{f_k}{f_{s,k}}\right)^2\right]} \tag{9}$$

$$Z_{TE} = \sqrt{\frac{\mu_o}{\epsilon_o}\frac{1}{\left(1-\left(\frac{f_k}{f_{s,k}}\right)^2\right)}} \tag{10}$$

where $f_{s,k}$ is the signal generator frequency that excites the kth mode. The signal excites both transverse magnetic (TM) and transverse electric (TE) modes within the resonant cavity. As the frequency $f_{s,k}$ approaches f_k, the impedance of the TM mode approaches zero, whereas the impedance of the TE mode becomes infinite. The presence of the TM mode at f_k reduces the cavity's efficiency due to increased I^2R losses. TE modes have the potential to induce arcing. Therefore, it is advisable to maintain $f_{s,k}$ at a distance from f_k to enhance efficiency. Magnetrons, with their broader bandwidth, are more effective in managing losses and arcing compared to solid-state alternatives. The modes within the cavity influence impedance. Introducing a sample under test (SUT) into the cavities alters the resonant frequencies, leading to impedance mismatches and increased power reflection back to the generators. In such scenarios, while spectral purity remains important, aligning the generator's frequency with the cavity's resonant frequencies is equally critical.

3. MATERIALS AND METHODS

Two domestic ovens of the same size were selected, with dimensions shown in Figure 4 and a volume given as 280 mm × 310 mm × 190 mm. The first, Oven 1, is a SAMSUNG Model *MW73AD-B/XTL* manufactured in 2017, while the second, Oven 2, is an IFB 24PM2B model acquired in 2024. Table 2 presents the comprehensive parameters of the two examined domestic microwave ovens. The mathematical analysis of the resonant modes within both cavities will be covered in Section 4. The materials and equipment used for the experimentation are listed in Table 3.

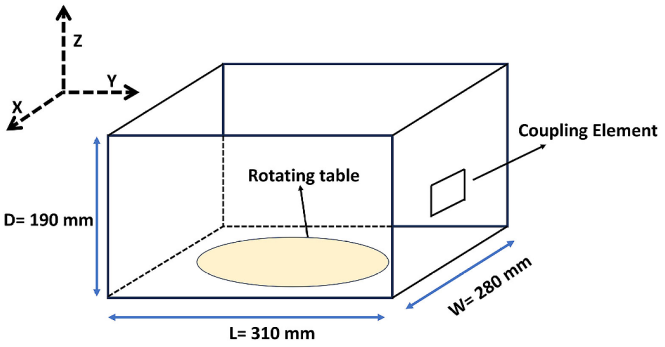

FIGURE 4. Microwave rectangular cavity dimensions.

3.1. Methodology

The method expands on prior research by investigating resonant modes within ovens [13–15], as shown in Figure 5. A probe designed at 2.45 GHz for a return loss greater than 10 dB tested the spectrum. It was connected to R&S spectrum analyser (SA) and placed 5 cms from the cavity door towards the magnetron side within a laboratory environment, as access to an anechoic chamber was not feasible. A wet thermal paper plotting is used for experimental investigations as documented by Kharkovsky and Hasar [24]. The time to raise the temperature of wet thermal paper by 100°C is approximately 30 secs [24]. Measurements were performed for both ovens during 60 secs

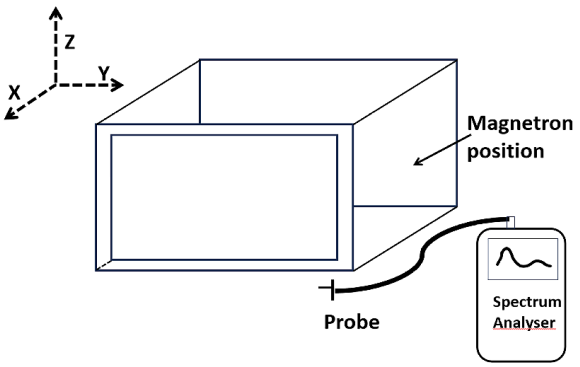

FIGURE 5. Spectral analysis measurement setup.

TABLE 3. Equipment/Material table for experimentation.

Equipment	Model/Spec	Purpose
Spectrum Analyser	Rohde & Schwarz FSH8	Spectrum Analysis
Microwave Cable	50 Ω frequency upto 3 GHz	to connect SA to probe
Probe	Designed and calibrated for return loss above 10 dB from 2.4 GHz to 2.5 GHz	Microwave pickup from the microwave oven for spectral analysis
Expanded Polyethylene (EPE) foam	1 inch thick	Support to place thermal paper and load
Thermal paper	Seznik A4 Thermal roll	Thermal plots
EM Simulation	Frequency domain solver, mesh density of 10 cells per max model box edge, boundary type is perfect electric	Cavity field distribution of modes inside the oven

heating in empty and loaded states, and the experimental heating patterns are observed using thermal paper supported over EPE foam due to the unavailability of thermal cameras. To investigate the modes within cavities when they are empty, wet thermal paper supported by EPE foam was placed in the ovens, and spectral measurements were conducted.

In empty cavity:

The spectral measurements enabled the identification of the resonant modes active during heating. The identified modes in both empty ovens were mathematically superimposed to assess their alignment with the experimental results.

For loaded cavity:

For the loaded cavity, a slice of bread was utilized, and to document electric field interactions with the load, moist thermal paper was positioned over the bread slice in both ovens. Spectral measurements were taken during the heating of the load, and an evaluation was performed to determine the spectral proximity to the resonant frequencies of the cavity. The experimental findings closely corresponded with the simulated results for the specified frequency. The simulation images and experimental thermal plot images were subsequently employed to analyze the Normalized Root Mean Squared Error (NRMSE). Equation (11) illustrates the use of NRMSE to quantify the discrepancies between experimental data and simulated results [30].

$$\text{NRMSE} = \sqrt{\frac{\sum(t_i - e_i)^2}{N}} \Big/ \frac{\sum(t_i + e_i)}{N} \qquad (11)$$

where t_i represents the data point from the simulated result image, and e_i represents the data point from the experimental result image. Errors due to spatial misalignment were corrected using image phase correlation; camera exposure mismatches were addressed by dark region linear rescaling; and background noise was corrected through 'hotspot only' analysis. The superposition of identified modes facilitated the prediction of heating patterns in magnetron-operated ovens.

4. EM SIMULATION RESULTS

The cavity coupled with a waveguide applicator is simulated to analyse mode presence over the spectrum from 2.4 to 2.5 GHz.

TABLE 4. List of analytical resonant frequencies and simulated signal frequencies of the rectangular empty microwave cavity.

m	n	p	Mode	f_r GHz	$f_{s,k}$ GHz
1	5	1	TE, TM	(f_1) 2.434	$(f_{s,1})$ 2.432
4	0	2	TE	(f_2) 2.457	$(f_{s,2})$ 2.455
3	4	1	TE, TM	(f_3) 2.462	$(f_{s,3})$ 2.460
3	3	2	TE, TM	(f_4) 2.479	$(f_{s,4})$ 2.476
2	5	0	TM	(f_5) 2.483	$(f_{s,5})$ 2.484
4	1	2	TE, TM	(f_6) 2.499	$(f_{s,6})$2.494

Results indicate the existence of six modes at $f_{s,k}$ within the spectrum, with details tabulated in Table 4. The computed frequency, f_r, evaluated using Equation (2), is close to mode frequencies, $f_{s,k}$, obtained by simulation. The resonant frequencies f_r are evaluated using Equation (2) and are close to mode frequencies $f_{s,k}$ obtained by simulation. As discussed in Section 2.1, multiple resonant frequencies in the cavity excite multiple modes. The resonances can be closely spaced, leading to adjacent mode excitations. It depends on the bandwidth of the magnetron and cavity quality factor [17]. The operational bandwidth of a magnetron increases as it ages, varying from 20 MHz to 70 MHz [15]. If the cavity has resonant frequencies closely spaced, a magnetron's large bandwidth can trigger multiple series resonant circuits, causing several modes to exist simultaneously. However, if cavity dimensions have resonant frequencies spaced greater than 10 MHz, adjacent modes will not be excited by a magnetron source. For discussion, we assume a magnetron with the least spectral bandwidth (i.e., 20 MHz) and a high Q factor of the cavity, and then the separation between adjacent f_r must be greater than 10 MHz to prevent the excitation of two modes. The simulated mode patterns as shown in Figure 6 are analysed at six frequency points, $f_{s,k}$. If the resonant frequencies are very close to each other, the excited mode pattern of any of them lacks clarity in any of the dimensions. This can be observed in Figure 6(b) and Figure 6(c), where $f_2 = 2.457$ GHz and $f_3 = 2.462$ GHz have a separation of 5 MHz. At f_2, the pattern is TE_{402} while the observed pattern is TE_{341}/TM_{341}, which is similar to that observed at f_3. In the mode excited at $f_{s,3}$, the pattern along the Z dimension lacks clarity as seen in Figure 6(c). In particular cases where modes

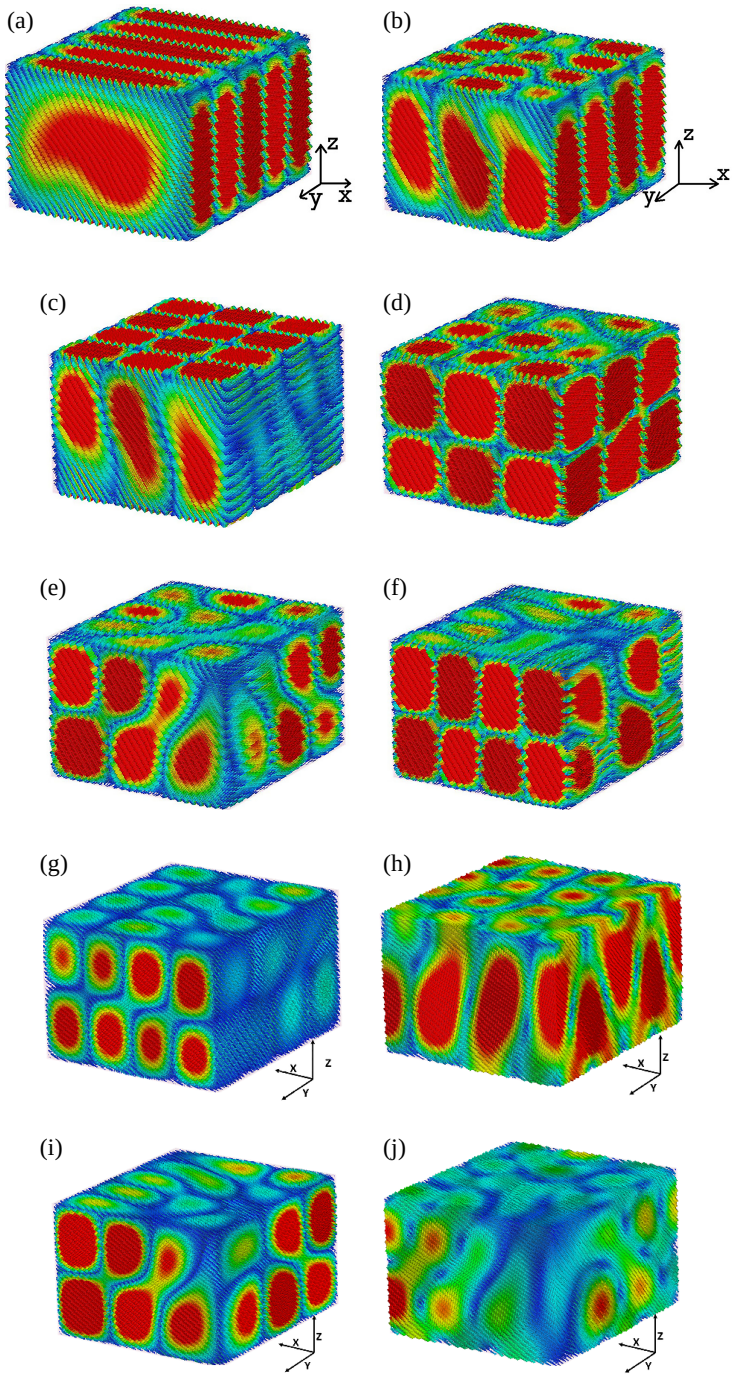

FIGURE 6. Field patterns inside the cavity from 2.4 GHz to 2.5 GHz at simulated frequency points. (a) Mode TE_{151} or TM_{151} ($f_1 = 2.434$ GHz) at $f_{s,1} = 2.432$ GHz. (b) Mode TE_{341} or TM_{341} ($f_2 = 2.457$ GHz) at $f_{s,2} = 2.455$ GHz. (c) Mode TE_{341} or TM_{341} ($f_3 = 2.462$ GHz) at $f_{s,3} = 2.460$ GHz. (d) Mode TE_{332} or TM_{332} ($f_4 = 2.479$ GHz) at $f_{s,4} = 2.476$ GHz. (e) Mode TE_{332} or TM_{332} ($f_5 = 2.479$ GHz) at $f_{s,5} = 2.484$ GHz. (f) Mode TE_{412} or TM_{412} ($f_6 = 2.499$ GHz) at $f_{s,6} = 2.494$ GHz. (g) Combined mode (TE_{402} & TE_{341}) at 2.457 GHz. (h) Mode TM_{341} at 2.457 GHz. (i) Combined TE mode (TE_{332} & TE_{250}) 2.483 GHz. (j) Combined TM mode at 2.483 GHz.

exhibit a unique configuration, such as TE_{402} mode, a remarkably high impedance is noted, as demonstrated in Equation (10). This phenomenon arises when the mode is excited close to its resonant frequency, resulting in impedance mismatches and a reduction in the power transferred to the cavity. Consequently, its TM counterpart, referred to as TE_{402}, is not visible with only the TE_{341} mode at 2.457 GHz observable in Figure 6(h). TE_{402} is clearly visible in the X-Z and Y-Z planes of Figure 6(g), while in the X-Y plane, there are conflicting patterns, suggesting the formation of the next mode, i.e., TE_{341}. Similarly, in another special mode, in Table 1 at $f_5 = 2.483$ GHz, the TM_{250} is expected but TE_{332} of $f_4 = 2.479$ GHz is observed since f_4 and f_5 are spaced by 4 MHz. As shown in simulation results, Figure 6(e) shows the presence of the TE_{332} at 2.484 GHz, and Figure 6(i) shows the appearance of the mode TE_{250} at 2.483 GHz (the top X-Y plane). The TM_{250} has a low

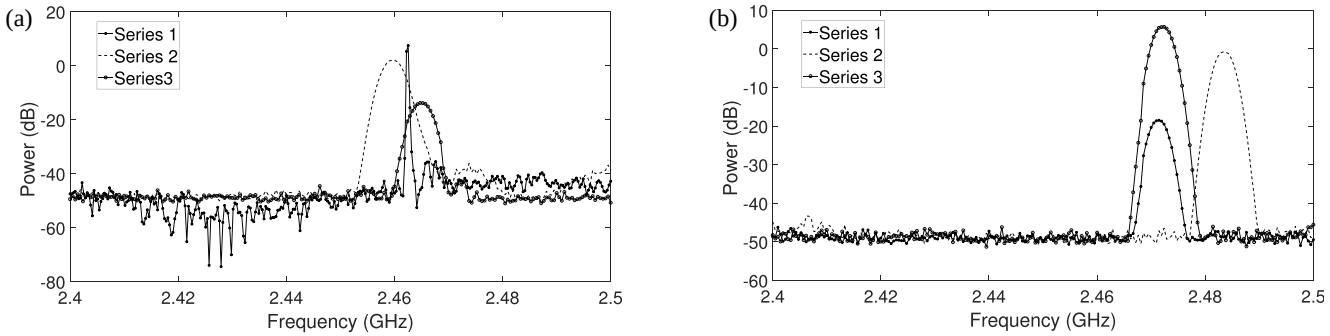

FIGURE 7. Spectrum of modes inside empty ovens. (a) Spectrum inside Empty Oven 1. (b) Spectrum inside Empty Oven 2.

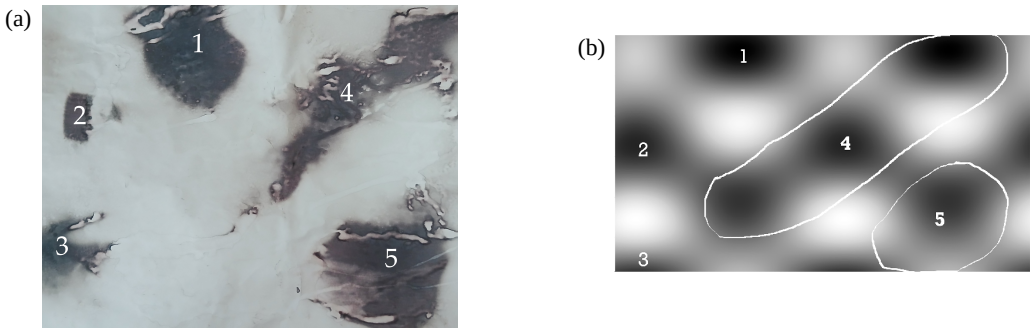

FIGURE 8. Mathematical analysis and experimental results of modes excited by the magnetron in the empty cavity of Oven 1. (a) Experimental analysis in Oven 1. (b) Mathematical analysis of two modes in Empty Oven 1.

impedance as shown by Equation (9), thereby reducing the efficiency of this mode at the resonant frequency and rendering its weak presence. The modes at $f_r = 2.434$ GHz, 2.462 GHz, 2.479 GHz, and 2.499 GHz appear as per the expected modes as shown by Figures 6(a), 6(c), 6(d) & 6(f), respectively. The coexistence of multiple modes depends on the spectrum of the induced signal, the matching of the impedance for various modes with the waveguide applicator, as well as the Q factor of the cavity. The mode TE_{412}/TM_{412} has discrepancies along the Y axis over the YZ plane, which could be due to the influence of forthcoming modes or due to the limitations of the bandwidth of the waveguide applicator, it can be further analysed for better clarity.

5. SIMULATION AND EXPERIMENTAL RESULTS IN MICROWAVE OVENS

In Oven 1 & Oven 2, spectral measurements were made as mentioned in Section 3.1. The spectral measurements were recorded consistently over a period of 60 secs with the turntable off, and the most consistent spectral images in the duration are shown over the observation period.

5.1. Simulation and Experimental Results in Empty Cavity

As illustrated in Figure 7(a), Empty Oven 1 consistently demonstrated frequencies at 2.458 GHz, 2.46 GHz, and 2.468 GHz across three series. Conversely, Empty Oven 2, with the turntable off, exhibited three spectral series, designated as Series 1, Series 2, and Series 3, at 2.473 GHz, 2.476 GHz, and 2.483 GHz, as depicted in Figure 7(b). As seen in Table 1, the listed modes TE_{402} & TE_{341} will be present in Oven 1 and the modes TE_{341} and TE_{250} for Oven 2 for the cavity under study, and hence these modes are to be superimposed to predict heating patterns in empty cavity of Oven 1 and Oven 2, respectively. The identified modes are TE_{402} & TE_{341} formed on thermal paper plot during experimentation and mathematically in X-Y plane are shown in Figures 8(a) and (b), respectively. The thermal paper plots are well formed, and they closely resemble those experimentally formed. The mathematical analysis of the two modes in Oven 2 and the experimental analysis prove that there is close agreement between the two results. The superposition of the 2 modes TE_{332} and TE_{250} within the cavity was mathematically computed and is shown in Figures 9(a) & 9(b). The grey or black areas on the thermal paper represent high microwave power deposited spots that cause heating, thereby darkening the areas, while those spots with no darkening have no or little heating. The comparative analysis of the experimentally obtained data & the mathematically computed data proves that the superposition of modes within the empty cavity of both ovens provides a better understanding of the heating patterns inside magnetron-based cavities.

5.2. Simulation and Experimental Results with Load in Cavity

Bread was placed inside the oven centre, and the frequency distributions were observed for both ovens. Oven 1 shows the specified 2.45 GHz spectrum as seen in Figure 10(a). As expected, the loading of the cavity results in shifting the modes

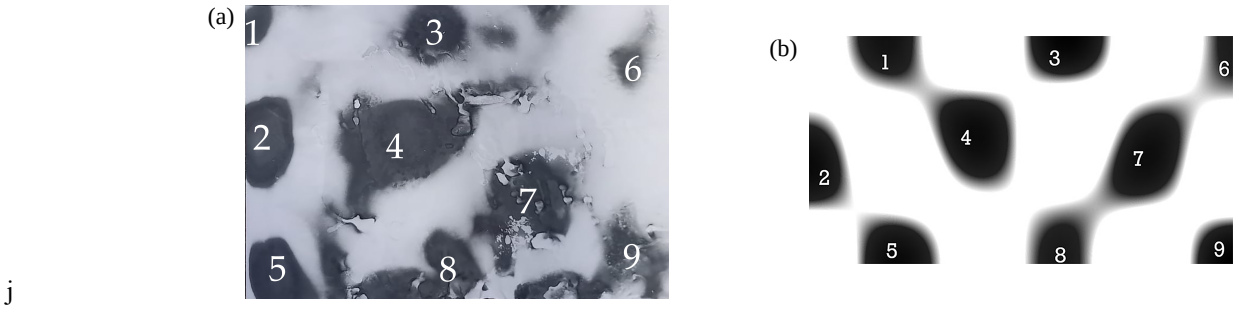

j

FIGURE 9. Mathematical analysis and experimental results of modes excited by the magnetron in the empty cavity in Oven 2. (a) Experimental analysis in Empty Oven 2. (b) Mathematical analysis of 2 modes in Oven 2.

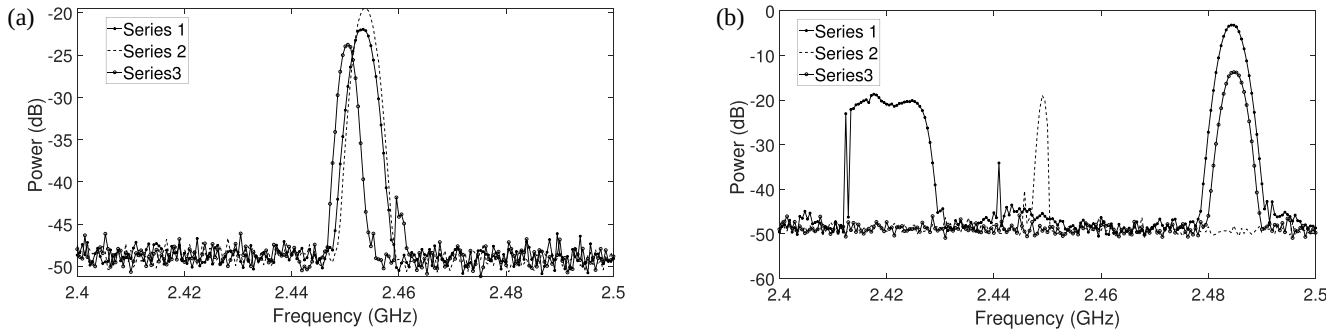

FIGURE 10. Spectrum of modes inside loaded ovens. (a) Frequency spectrum with bread in Oven 1. (b) Frequency spectrum with bread in Oven 2.

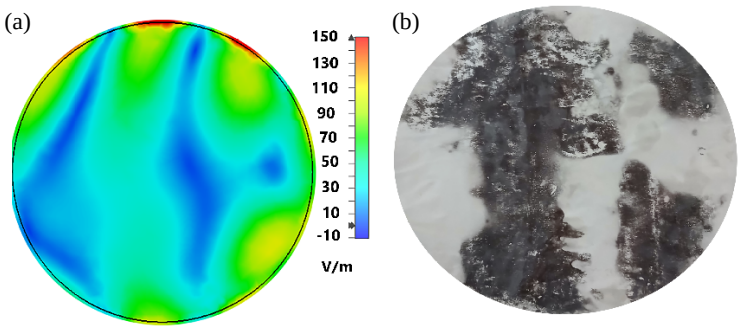

FIGURE 11. Simulated & experimental results on the surface of bread in Oven 1. (a) Simulated E field over surface of bread at 2.457 GHz. (b) Experimental E field over surface of bread.

lower, as compared with Figure 7(a), where the peak observed is at frequency 2.457 GHz. Similarly, as seen in Figure 10(b), for Oven 2, the frequency spectrum with low peaks is observed near 2.42 GHz, while the one with high peaks is observed at 2.485 GHz. The results of the EM simulation were derived with the consideration of bread. The specific heat associated with bread, utilized for theoretical examination, is sourced from the work of Zheleva and Kambourova [31]. In this material analysis, a slice of bread weighing 90 grams occupies an approximate volume of 251 cm^3. The subsequent assumptions are established to facilitate a deeper discussion and comprehension of the experimental outcomes. The specific heat, c_p, of bread is 2890 Joule $(kg°C)^{-1}$. The effective dielectric constant, ϵ_{eff}, is taken as 14.37 at room temperature using estimated dielectric values of solid bread material from Liu et al. [32], where $\epsilon_{eff} = (\epsilon_r^{''} + \frac{\sigma}{\omega\epsilon_o})$ [17], $\omega = 2\pi f$, and σ is the electrical conductivity.

In Oven 1, since the loaded cavity reveals a frequency of 2.457 GHz, the simulated results at 2.457 GHz are presented in Figure 11(a). The experimental findings from Oven 1, illustrated in Figure 11(b), exhibit cold spots that are grey/white corresponding to the blue locations indicated by the simulated pattern shown in Figure 11(a). The cold spot locations are identical to the low electric (E) field locations, while in regions where the E field is high, the heat induced will spread through the material depending upon the heat transfer rate of the material. The discrepancies arise because the model parameters for bread are not sufficiently documented in the literature for an accurate EM simulation setup. The EM simulation data over bread for Oven 2, depicted in Figure 12(a), was collected at

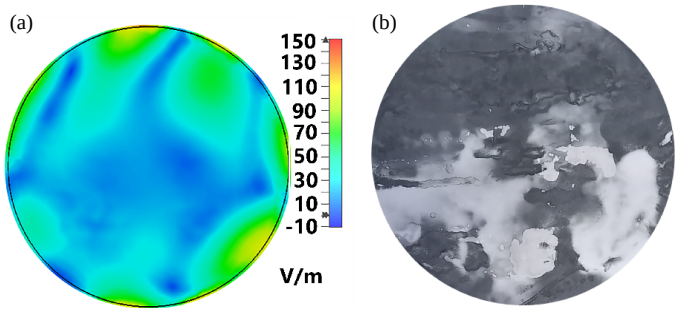

FIGURE 12. Simulated & experimental results on the surface of bread in Oven 2. (a) Simulated E field over surface of bread at 2.485 GHz. (b) Experimental E field over surface of bread.

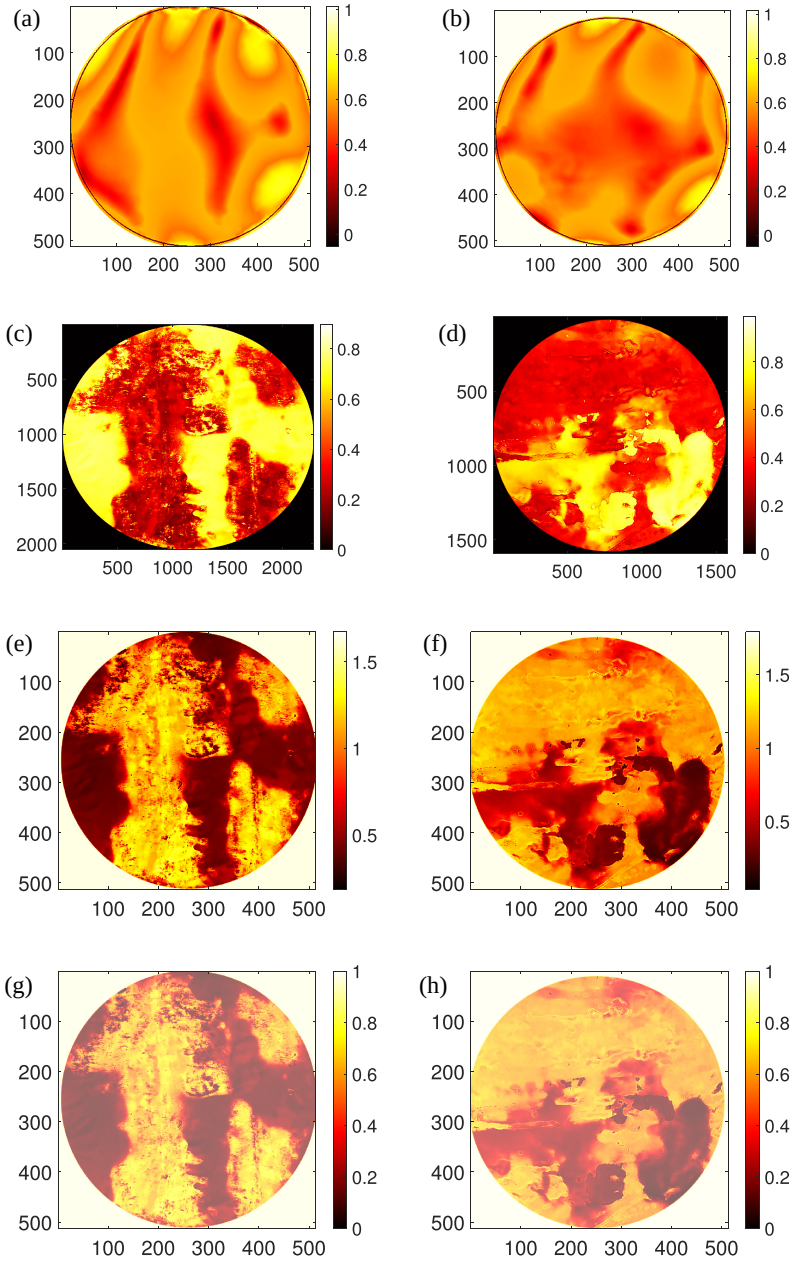

FIGURE 13. Statistical agreement analysis of simulation and experimental results in Oven 1 and Oven 2. (a) Simulated results in Oven 1. (b) Simulated results in Oven 2. (c) Experimental − Black = High results in Oven 1. (d) Experimental − Black = High results in Oven 2. (e) Experimental rescaled dark μ match = 0% Oven 1. (f) Experimental rescaled dark μ match = 0% Oven 2. (g) Overlay $r = -0.451$ & NRMSE = 0.194. (h) Overlay $r = 0.039$ & NRMSE = 0.075.

a frequency of 2.485 GHz, as this frequency corresponds to the highest peak, with other peaks being significantly lower, as evidenced in Figure 10(b). The experimental findings from Oven 2, illustrated in Figure 12(b), exhibit cold spots that are grey/white corresponding to the blue locations indicated by the simulated pattern shown in Figure 12(a). There is a strong correlation observed between simulated and experimental results of the field pattern over the bread surface in Oven 2.

The statistical analysis of both experimental and simulated outcomes revealed a strong concordance, as illustrated in Figure 13, with a standard deviation of $\mu = 0\%$ in both ovens. Various preprocessing stages are depicted, wherein the darker regions of the experimental data were aligned, rescaled, and normalized to correspond to the intensity levels of the simulated results, as shown in Figures 13(e) and 13(f). Additionally, the hotspot areas underwent subpixel adjustments, with the NRMSE for Oven 1 recorded at 0.194 and for Oven 2 at 0.075, respectively, reflecting a close agreement between the obtained results.

6. CONCLUSION

The research indicates a significant relationship between the field patterns produced across the loading plane within a domestic oven. The data pertaining to the dimensions of the cavity, along with the frequency spectrum generated by the magnetron, is adequate for forecasting heating distributions on the surface of the SUT. The model parameters of the SUT are crucial in determining the diffusivity of heat and depth of penetration throughout its medium, and consequently, obtaining precise information regarding these parameters can enhance predictive accuracy. When magnetrons operating at various frequencies are positioned within expansive cavities used for batch processing materials, they can effectively excite successive modes, thus promoting more uniform heating. This scenario allows for the development of specific selection criteria for magnetrons to achieve optimal heating performance.

REFERENCES

[1] Bradshaw, S., S. Delport, and E. van Wyk, "Qualitative measurement of heating uniformity in a multimode microwave cavity," *Journal of Microwave Power and Electromagnetic Energy*, Vol. 32, No. 2, 87–95, 1997.

[2] Ye, J., C. Zhang, and H. Zhu, "A temperature-control system for continuous-flow microwave heating using a magnetron as microwave source," *IEEE Access*, Vol. 8, 44 391–44 399, 2020.

[3] Monzó-Cabrera, J., J. L. Pedreño-Molina, and A. Toledo, "Feedback control procedure for energy efficiency optimization of microwave-heating ovens," *Measurement*, Vol. 42, No. 8, 1257–1262, 2009.

[4] Song, Y., H. Pan, L. Ge, L. Qiu, S. Kumar, and Y.-C. Chen, "Microsurf: Guiding energy distribution inside microwave oven with metasurfaces," in *Proceedings of the 30th Annual International Conference on Mobile Computing and Networking*, 1346–1360, Washington D.C., USA, 2024.

[5] Yang, R., A. E. Fathy, M. T. Morgan, and J. Chen, "Development of online closed-loop frequency shifting strategies to improve heating performance of foods in a solid-state microwave system," *Food Research International*, Vol. 154, 110985, 2022.

[6] Chen, S., S. Cen, R. Liu, C. Tao, S. Guo, and G. Chen, "Microwave reactor with combined rigid and flexible stirring paddles for improving fluid heating uniformity in soft manganese Ore leaching processes," *ACS Omega*, Vol. 8, No. 45, 42 367–42 378, 2023.

[7] Guzik, P., P. Kulawik, M. Zając, and W. Migdał, "Microwave applications in the food industry: An overview of recent developments," *Critical Reviews in Food Science and Nutrition*, Vol. 62, No. 29, 7989–8008, 2022.

[8] Yang, B., H. Huang, L. Zhou, and H. Jin, "Method for solving the microwave heating temperature distribution of the TE_{10} mode," *Processes*, Vol. 10, No. 7, 1377, 2022.

[9] Su, T., W. Zhang, Z. Zhang, X. Wang, and S. Zhang, "Energy utilization and heating uniformity of multiple specimens heated in a domestic microwave oven," *Food and Bioproducts Processing*, Vol. 132, 35–51, 2022.

[10] Pitchai, K., S. L. Birla, D. Jones, and J. Subbiah, "Assessment of heating rate and non-uniform heating in domestic microwave ovens," *Journal of Microwave Power and Electromagnetic Energy*, Vol. 46, No. 4, 229–240, 2012.

[11] Ahn, S.-H., C.-H. Jeong, D.-M. Lim, and W.-S. Lee, "Kilowatt-level power-controlled microwave applicator with multiple slotted waveguides for improving heating uniformity," *IEEE Transactions on Microwave Theory and Techniques*, Vol. 68, No. 7, 2867–2875, 2020.

[12] Hill, D. J., C. D. Rudd, and M. S. Johnson, "Design and application of a cylindrical TM_{020} mode applicator for the in-line microwave preheating of liquid thermosets," *Journal of Microwave Power and Electromagnetic Energy*, Vol. 33, No. 4, 216–230, 1998.

[13] Birla, S., K. Pitchai, J. Subbiah, and D. D. Jones, "Effect of magnetron frequency on heating pattern in domestic oven," in *International Microwave Power Institute's 44th Annual Symposium*, Denver, Colorado, USA, 2010.

[14] Luan, D., Y. Wang, J. Tang, and D. Jain, "Frequency distribution in domestic microwave ovens and its influence on heating pattern," *Journal of Food Science*, Vol. 82, No. 2, 429–436, 2017.

[15] Zhou, X., P. D. Pedrow, Z. Tang, S. Bohnet, S. S. Sablani, and J. Tang, "Heating performance of microwave ovens powered by magnetron and solid-state generators," *Innovative Food Science & Emerging Technologies*, Vol. 83, 103240, 2023.

[16] Zhou, X., Z. Tang, P. D. Pedrow, S. S. Sablani, and J. Tang, "Microwave heating based on solid-state generators: New insights into heating pattern, uniformity, and energy absorption in foods," *Journal of Food Engineering*, Vol. 357, 111650, 2023.

[17] Meredith, R. J., *Engineers' Handbook of Industrial Microwave Heating*, 1–192, IET, 1998.

[18] Barham, J. P., E. Koyama, Y. Norikane, N. Ohneda, and T. Yoshimura, "Microwave flow: A perspective on reactor and microwave configurations and the emergence of tunable single-mode heating toward large-scale applications," *The Chemical Record*, Vol. 19, No. 1, 188–203, 2019.

[19] Carvalho, F., A. Kotrashetti, and K. Bhattacharyya, "Investigation of heating in microwave cavities: Insights, evolution, and advancements," *IETE Journal of Research*, 1–16, 2025.

[20] Nott, K. P., L. D. Hall, J. R. Bows, M. Hale, and M. L. Patrick, "Three-dimensional MRI mapping of microwave induced heating patterns," *International Journal of Food Science and Technology*, Vol. 34, No. 4, 305–315, 1999.

[21] Antuono, C., L. Sito, E. Calzone, D. El Dali, M. Migliorati, A. Mostacci, V. R. Marrazzo, G. Breglio, G. Rumolo, and C. Zannini, "A novel approach for measuring transverse beam-coupling impedance in particle accelerator systems utilizing the

bead-pull technique," *IEEE Transactions on Instrumentation and Measurement*, Vol. 73, 1–9, 2024.

[22] Sun, M. H., K. A. Wickersheim, A. Kamal, and W. R. Kolbeck, "Fiberoptic sensor for minimally-perturbing measurement of electric fields in high power microwave environments," *MRS Online Proceedings Library*, Vol. 189, No. 1, 141–145, 1990.

[23] Ng, K. H., "Microwave ovens: Mapping the electrical field distribution," *Medical Laboratory Sciences*, Vol. 48, No. 3, 189–192, 1991.

[24] Kharkovsky, S. N. and U. C. Hasar, "Measurement of mode patterns in a high-power microwave cavity," *IEEE Transactions on Instrumentation and Measurement*, Vol. 52, No. 6, 1815–1819, 2003.

[25] Metaxas, A. C. and R. J. Meredith, *Industrial Microwave Heating*, 4–67, IET, 1983.

[26] Tian, W., X. Feng, L. Gao, K. Chen, Y. Chen, J. Shi, and H. Lao, "Improvement of microwave heating uniformity using symmetrical stirring," *Symmetry*, Vol. 17, No. 5, 659, 2025.

[27] Mehdizadeh, M., *Microwave/RF Applicators and Probes: For Material Heating, Sensing, and Plasma Generation*, 2nd ed., 1–363, William Andrew, 2015.

[28] Hazervazifeh, A., A. M. Nikbakht, and S. Nazari, "Industrial microwave dryer an effective design to reduce non-uniform heating," *Engineering in Agriculture, Environment and Food*, Vol. 14, No. 4, 110–121, 2021.

[29] Weng, Y.-K., J. Chen, C.-W. Cheng, and C. Chen, "Use of modern regression analysis in the dielectric properties of foods," *Foods*, Vol. 9, No. 10, 1472, 2020.

[30] James, G., D. Witten, T. Hastie, and R. Tibshirani, *An Introduction to Statistical Learning: With Applications in R*, Vol. 103, Springer, 2013.

[31] Zheleva, I. and V. Kambourova, "Identification of heat and mass transfer processes in bread during baking," *Thermal Science*, Vol. 9, No. 2, 73–86, 2005.

[32] Liu, Y., J. Tang, and Z. Mao, "Analysis of bread dielectric properties using mixture equations," *Journal of Food Engineering*, Vol. 93, No. 1, 72–79, 2009.